Journal of Electronic Materials
https://doi.org/10.1007/s11664-024-11146-1

ORIGINAL RESEARCH ARTICLE

High-Performance Ammonia Detection of Polymeric $BaTiO_3/Ti_3C_2T_x$ MXene Composite-Based Sensor for Gas Emission and Leakage

Guoqing Sun[1] · Chenglin Wang[1] · Jie Jia[1] · Hao Zhang[2] · Yaqing Hu[2] · Yukun Liu[2] · Dongzhi Zhang[2]

Received: 6 February 2024 / Accepted: 25 April 2024

Abstract

NH_3 is a dangerous gas, posing significant threats to human health and the delicate equilibrium of the environment. It emerges as a primary contributor to the noxious gas emissions prevalent in the selective catalytic reduction (SCR) processes employed by marine diesel engines. Its deleterious impact extends beyond the immediate surroundings, permeating the air with potential health hazards and exacerbating environmental degradation. The repercussions of NH_3 emissions are far-reaching, impacting respiratory health, ecosystem vitality, and overall air quality. In this paper, $BaTiO_3/Ti_3C_2T_x$ composites were synthesized by anchoring $BaTiO_3$ nanospheres on multilayer $Ti_3C_2T_x$ nanosheets. The shortcomings of low sensitivity and poor recovery of the pristine $Ti_3C_2T_x$ MXene gas sensor were improved. The $BaTiO_3$/MXene composite sensor exhibits an improved response (10.43) to 20 ppm NH_3 at room temperature, which is about 3.5 times higher than that of the pure MXene sensor. Furthermore, the $BaTiO_3$/MXene composite sensor greatly improves the recovery time and exhibits outstanding repeatability, stability, and high selectivity to NH_3. The exceptional characteristics of these composites underscore the potential for advancing novel sensitive materials in the form of $BaTiO_3$/MXene composites, specifically tailored for high-performance NH_3 sensors.

Keywords Ammonia gas sensor · MXene nanosheet · $BaTiO_3$ nanosphere · selective catalytic reduction

Introduction

In recent years, the leakage of volatile toxic gases and steam generated by chemical combustion and chemical reactions in a wide range of industrial production and other fields has caused pollution to the environment and also poses a serious threat to human health.[1,2] Pollution gas emissions produced by marine diesel engines bring great harm to the human living environment and physical health. In order to meet strict ship emissions restrictions and to reduce pollution and harm to the atmosphere, selective catalytic reduction (SCR) technology is widely used in ships, so the detection of SCR emissions from marine diesel engines is of great research significance. Ammonia (NH_3) is one of the gases harmful to human health and the environment, and is also one of main components of pollution gas emissions in selective catalytic reduction (SCR) from marine diesel engines. Furthermore, NH_3 is also an important indicator for the diagnosis of diabetes, malignant tumors, lung cancer, kidney disease, and other diseases.[3] For example, the concentration of NH_3 in exhaled breath is about 0.8 ppm in healthy individuals, while this increases to more than 1.5 ppm in patients with kidney disease. Although NH_3 has many uses, it is a colorless, toxic, and pungent gas that poses a threat to human health. For example, prolonged exposure to a certain concentration of NH_3 can elicit irritation on the skin, eyes, and respiratory system, potentially causing burns. Human exposure to 35 ppm NH_3 gas for 15 min will cause cell damage. Excessive NH_3 inhalation in a short period of time may cause lung and throat swelling, and in severe cases may lead to necrosis and detachment of bronchial mucosa, eventually leading to asphyxia.[3–6] Therefore, the assessment of NH_3 gas concentration holds considerable significance, and it is a challenging and urgent task to explore and design new materials suitable for NH_3 detection.

✉ Chenglin Wang
wangchenglin@cnijx.com

✉ Dongzhi Zhang

Hao Zhang
dzzhang@upc.edu.cn

[1] China Nuclear Power Maintenance Co., Ltd, Qingdao 266404, China

[2] College of Control Science and Engineering, China University of Petroleum (East China), Qingdao 266580, China

Published online: 11 May 2024

Among the many double-metal oxide semiconductor materials, barium titanate ($BaTiO_3$), as an environmentally friendly ceramic material with high dielectric constant, large charge storage capacity, and low loss current density, has great potential in the electronics industry.[7,8] Compared with other metal oxides, the advantages of using perovskite semiconductor $BaTiO_3$ sensors are high chemical stability, low cost, and simple structure.[9] Although barium titanate has been used to detect carbon dioxide, carbon monoxide, ammonia, hydrogen sulfide, and other gases, its low sensitivity and slow response/recovery speed have severely hindered its commercial application.[10,11] The performance of metal in sensing oxide nanostructures can be improved by changing the morphology of the material, doping with precious metals, or forming heterostructures through different preparation methods.[12] Among them, the combination of heterostructure materials is considered a very effective strategy. To the best of our knowledge, there is no documentation on the $BaTiO_3$/MXene heterostructure. This lack of existing information underscores its novelty and uniqueness, as it stands as an unexplored and uncharted domain in current scientific discourse.

Speaking broadly, the methodologies utilized for the preparation of $BaTiO_3$ are primarily centered around spray pyrolysis, the sol–gel approach, and the hydrothermal process. Compared with other preparation processes, the hydrothermal method possesses the benefits of low equipment cost, low process temperature, low cost, and easy particle size control.[13] Another advantage of preparing $BaTiO_3$ by hydrothermal synthesis is that it can reduce pollution, protect the environment, and can more easily control the morphology and size distribution of synthetic materials.[14] Research investigations have indicated that inducing diverse morphologies within a given material is crucial for augmenting its gas-sensing capabilities. This empirical evidence suggests that the creation of varied structural forms of the identical substance plays a pivotal role in elevating its sensitivity to gases.

MXenes represent a novel class of two-dimensional materials encompassing transition metal carbides, nitrides, and carbonitrides, holding expansive prospects for various applications. Among them, $Ti_3C_2T_x$[15,16] is frequently encountered. MXenes are usually prepared by etching layered ternary carbides or nitrides (MAX phase) and selectively etching "A" elements. The general formula is $M_{n+1}X_nT_x$.[17] For example, $Ti_3C_2T_X$ is obtained by etching Ti_3AlC_2 with HF aqueous solution at room temperature and selectively removing Al.[18,19] In the course of the etching procedure, hydrophilic $Ti_3C_2T_x$ nanosheets are produced, with T_x denoting diverse surface functional groups, including -OH, -O, and -F.[20–22] These active ends provide MXenes with abundant gas adsorption functional sites for the adsorption of analyte species.[23,24] In addition, due to its large specific surface area, excellent surface tunability, ultra-high metal conductivity, very narrow band gap, and fast electron transfer ability, it has proven to be a good gas sensing material.[25] Despite its many advantages, the sensitivity, selectivity and response/recovery time of MXenes still need to be improved. The combination of MXenes with metal oxides is proved to be an effective route to enhance the sensitivity of MXenes-based gas sensors.[26–28]

In order to develop a high-performance ammonia gas sensor, $BaTiO_3/Ti_3C_2T_x$ composites were synthesized by anchoring $BaTiO_3$ nanospheres on $Ti_3C_2T_x$ nanosheets. The sensor comprising the $BaTiO_3$/MXene composite exhibits a remarkable degree of sensitivity, noteworthy consistency, robust stability, and elevated selectivity when operated at room temperature. This composite sensor stands out for its ability to consistently and accurately detect changes in the environment, showing a high level of responsiveness that attests to its effectiveness in real-world applications. The excellent properties of the $BaTiO_3$/MXene composites demonstrate great potential of the $BaTiO_3$/MXene composite as building blocks for constructing NH_3 gas sensors in pollution gas detection.

Experimental

Synthesis of Delaminated $Ti_3C_2T_x$

The following are methods for preparing MXene and calculating the concentration of layered MXene dispersions. Layered $Ti_3C_2T_x$ MXene with good dispersibility in water was synthesized by etching Ti_3AlC_2 with an HCl/LiF mixed solution. Then, 1 g LiF was added to 20 mL of HCl solution with a concentration of 6 mol/L and stirred until completely dissolved. Next, 1 g Ti_3AlC_2 was slowly added to the above mixed acid solution and allowed to stand at 35 °C for 24 h. The reaction solution was subjected to consecutive rinses using deionized water and centrifugation procedures, continuing until the pH of the supernatant exceeded 6, resulting in the acquisition of a dispersion solution containing MXene. A small amount of MXene dispersion was vacuum-filtered, and the mass of the filtered MXene was measured to determine the concentration of the layered MXene dispersion.

Synthesis of Delaminated $BaTiO_3$

The following is the procedure for the preparation of $BaTiO_3$ powder. $Ba(OH)_2{\cdot}8H_2O$ was used as the barium precursor, and TiO_2 was used as the Ti precursor. First, around 1.577 g (5 mmol) of barium hydroxide octahydrate and 0.4 g (5 mmol) of titanium dioxide were introduced to a beaker with 30 mL of deionized water. To ensure the successful synthesis of $BaTiO_3$, the ratio of barium to titanium needs to

be maintained (Ba:Ti = 1). A certain amount of NaOH was added to the above solution to make the pH of the solution between 9 and 10, which ensures that the alkalinity of the aqueous solution is sufficient to precipitate $BaTiO_3$. Following this, the blend was moved to a 100-mL stainless steel autoclave coated with polytetrafluoroethylene and subjected to 100 °C heat for 48 h. Then, the obtained precipitate was washed alternately with deionized water and ethanol and centrifuged at 5000 rpm for 10 min to obtain a white precipitate. To eliminate any $BaCO_3$ impurities, it underwent treatment with 0.1 M formic acid at 30 °C for 2–3 h, followed by rinsing with deionized water 5–6 times. After that, it was dried at 75 °C for 12 h to obtain a white powder of $BaTiO_3$.

Production and Measurement of Gas Sensors

The structural characteristics of both the MXene and $BaTiO_3$/MXene nanocomposites were meticulously investigated using a scanning electron microscope (SEM; S-4800; Hitachi). In this examination, the morphology and microstructure of the materials were scrutinized with high precision and detail. The surface features and internal arrangements of the MXene and $BaTiO_3$/MXene nanocomposites were subjected to in-depth analysis through the utilization of the SEM, offering a comprehensive understanding of their physical attributes. X-ray diffraction (XRD; D/Max 2500 PC; Rigaku) was used to analyze the phase composition of the sample. The elemental composition of the sample was verified through x-ray photoelectron spectroscopy (XPS; K-α; Thermo Scientific), following the observation by high-resolution transmission electron microscopy (HRTEM; Tecnai F30; Philips). The MXene and $BaTiO_3$ were mixed to obtain the $BaTiO_3$/MXene composite. A certain amount of $BaTiO_3$ and MXenes were mixed and ground into powders, then poured into 20 mL of deionized water, treated with ultrasonics for 0.5 h and magnetic stirring for 2 h to form a $BaTiO_3$/MXene hybrid suspension. Finally, the $BaTiO_3$/MXene composite was obtained by drying the suspension under vacuum at 60 °C for 6 h. The prepared sample was mixed with ethanol to form a paste on the interdigital electrode and dried at 60 °C. Figure 1 illustrates the sensor's structural diagram with a diagram depicting its gas performance test.

A computer-controlled Agilent 34970A measured the resistance response of the prepared $BaTiO_3$/MXene nanocomposite sensor. Varied concentrations of NH_3 gas were achieved by evaporating distinct volumes of NH_3 aqueous solution, followed by the adsorption and removal of water vapor using activated carbon. In addition, air was used as the background gas (33% relative humidity; RH) in the experimental tests. The sensor's responsiveness, denoted as the sensor response (*S*), was determined by computing the ratio of the sensor resistance when exposed to NH_3 gas (Ra) to its resistance in ambient air (Rg). This quantitative metric encapsulates the sensor's ability to discern and react to the presence of NH_3, providing a reliable gauge of its detection efficacy. Providing further insight into the dynamic performance of the sensor, it is crucial to consider the response and recovery times as pivotal parameters. The response time signifies the duration required for the sensor to register a substantial alteration, reaching a point where 90% of the overall resistance change has been attained. Conversely, the

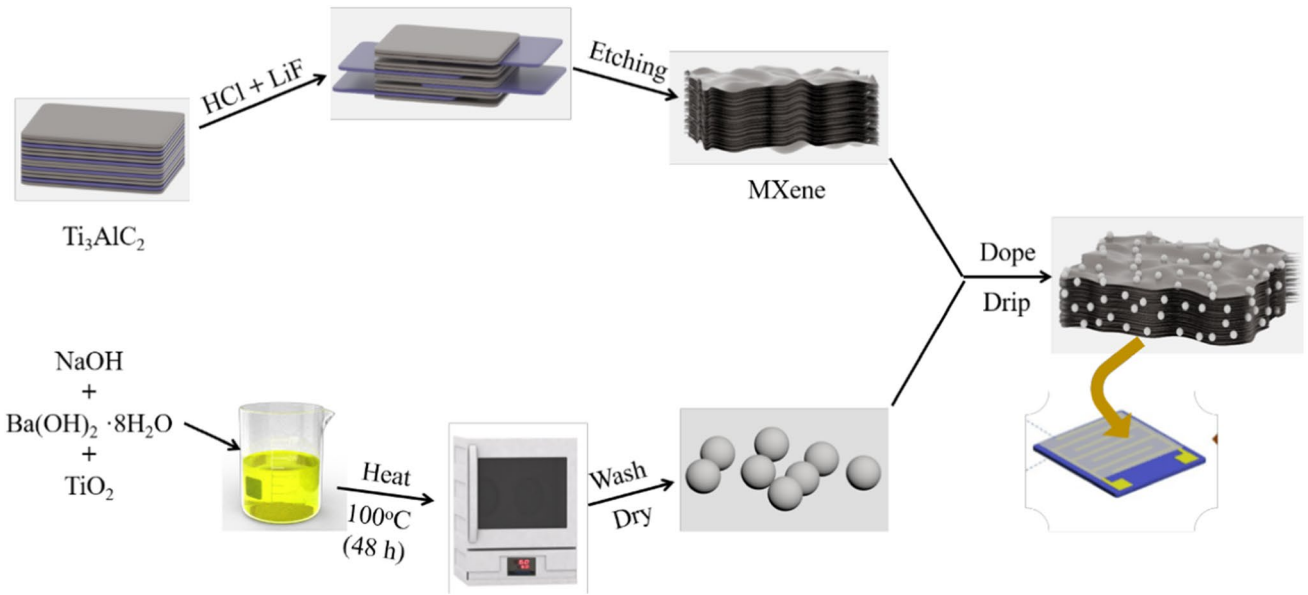

Fig. 1 Process flow chart of the preparation of $BaTiO_3$/MXene composite nanomaterials.

recovery time delineates the timeframe essential for the sensor to revert to its baseline resistance level following exposure to NH_3.

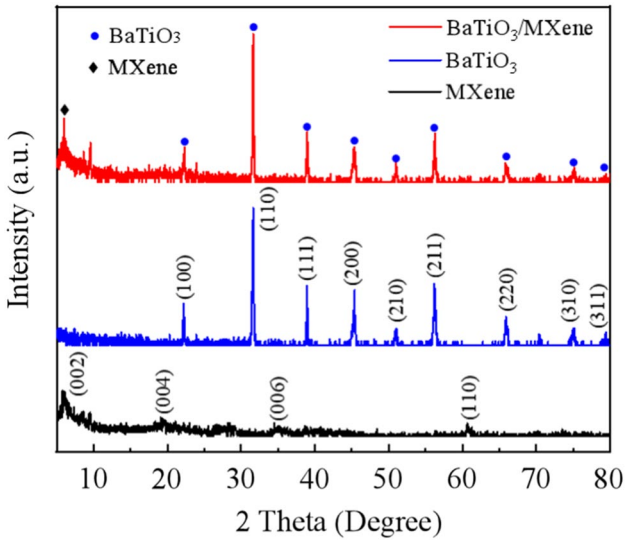

Fig. 2 XRD patterns of MXene, $BaTiO_3$, and $BaTiO_3$/MXene samples.

Results and Discussion

Characterization of Sensing Materials

The XRD patterns of the MXene, $BaTiO_3$, and $BaTiO_3$/MXene samples are shown in Fig. 2. The characteristic peaks located at the 2θ values of 22.16°, 31.62°, 38.94°, 45.36°, 51.06°, 56.26°, 65.86°, 75.02°, and 79.32° can be assigned to the (100), (110), (111), (200), (210), (211), (220), (300), (310), and (311) crystal planes, could be well indexed to the tetragonal structure of $BaTiO_3$ (JCPDS Card.#31-0174).[29,30] The diffraction peaks observed at 2θ values of 5.97°, 19.11°, 28.47°, and 60.27° in pure MXene correspond to the (002), (004), (006), and (110) crystal planes of MXene.[31] In the XRD analysis of the MXene/$BaTiO_3$ composite, the (002) peak of MXene exhibited a subtle shift towards the lower-angle region. This can be ascribed to the intercalation of Ba and Ti atoms within the interlayer spaces of MXene. No obvious other impurity peaks were observed, indicating that the purity of the prepared sample was excellent.

The structural characteristics and micro-architecture of the materials studied by SEM are shown in Fig. 3, where MXene presents an accordion-like layered structure. The $BaTiO_3$ nanospheres are uniformly distributed

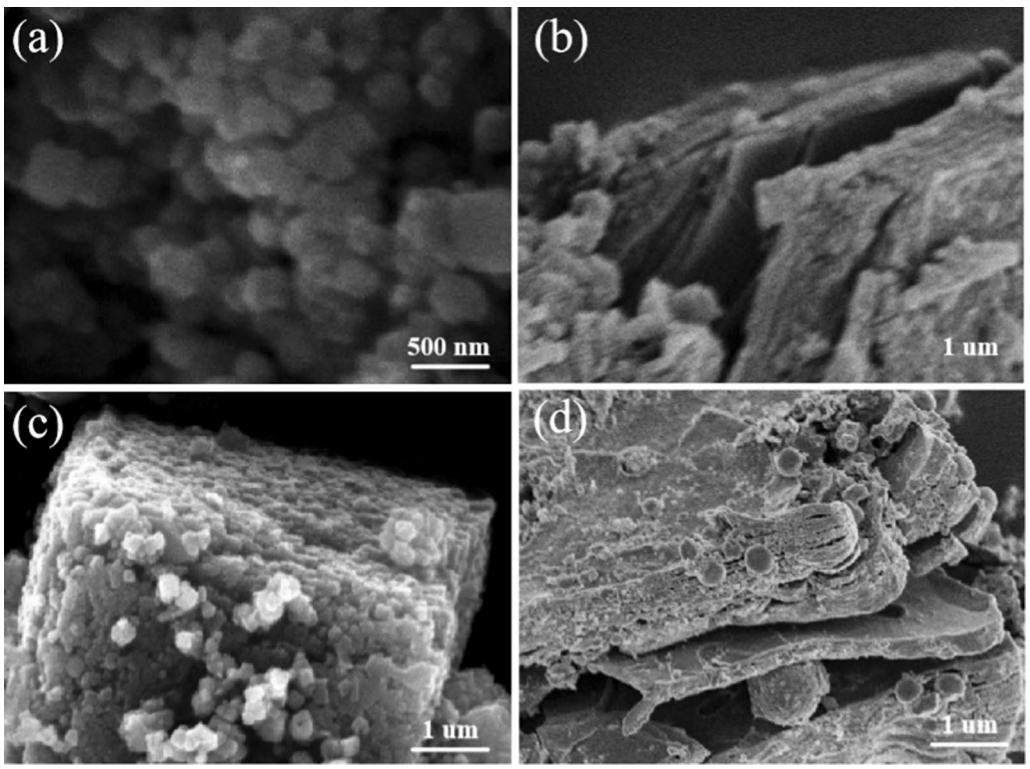

Fig. 3 (a) XRD patterns of $BaTiO_3$, MXene, and $BaTiO_3$/MXene samples. SEM images of (b) $BaTiO_3$ NFs, (c) MXene, and (d) $BaTiO_3$/MXene nanocomposite.

in the composite, and also randomly embedded between the MXene layers, which shows a good combination of MXene/$BaTiO_3$ nanocomposites.

Transmission electron microscopy (TEM) has been used to further study the morphology and microstructure of the samples, which are more conducive to analyzing them in principle as being high-performance sensors. From Fig. 4a and b, we can see the coexistence and combination of $BaTiO_3$ and MXene. Figure 4c and d shows the HRTEM images of the $BaTiO_3$/MXene sample, in which obvious boundaries between the two and clear lattice fringes can be seen., while the crystal plane spacing of $BaTiO_3$ (1 0 1) and MXene (0 0 6) are 0.28 nm and 0.25 nm, respectively.[32]

The XPS spectra of the $BaTiO_3$/MXene composite Ba 3*d*, C 1*s*, Ti 2*p*, and O 1*s* peaks can be observed in Fig. 5, which indicates that the composites are mainly composed of four elements, Ba, C, Ti, and O. As shown in Fig. 5a, the fitted peaks at 794.7 and 793.3 eV belong to Ba $3d_{5/2}$, while the fitted peaks at 779.4 and 777.6 eV correspond to Ba $3d_{3/2}$.[33] The four main peaks at 287.5, 285.3, 284.2, and 280.3 eV of the XPS spectrum of C 1*s* correspond to C=O, C-O, C-C, and C-Ti, respectively.[34] In addition, the XPS spectrum of Ti 2*p*, shown in Fig. 5c, can also be fitted to four main peaks. The binding energies at 463.4 and 458.2 eV may correspond to Ti $2p_{½}$ and Ti $2p_{3/2}$.[35] The other two peaks at 457.5 and 454.1 eV correspond to Ti-X(Ti^{+}) and Ti-C(Ti^{2+}). In Fig. 5d, the three characteristic peaks located at 528.4, 530.9, and 532.3 eV correspond to the Ti-O, C-Ti-(OH)x, and HO-Ti bonds, respectively.[36]

NH_3 sensing properties

Figure 6a shows the responses of a pristine $BaTiO_3$ sensor, a pristine MXene sensor, and a $BaTiO_3$/MXene composite nanomaterial sensor to different concentrations of NH_3 (25 °C, 33%RH). In the 0.5–40 ppm NH_3 gas environment, the response of the composite sensor is 2.01, 5.33, 14.44, 23.97, 36.91, 48.69, and 61.66, respectively. Compared with the pure $BaTiO_3$ sensor (21.12@20 ppm NH_3) and MXene sensor (10.43@20 ppm NH_3), the response of the $BaTiO_3$/MXene composite sensor is increased by about 1.7 times and 3.5 times. This is due to the synergy between the MXene nanosheets and the $BaTiO_3$ nanospheres, which has the potential to significantly enhance the sensing capabilities for NH_3. Figure 6b shows the fitting curve between the responses of pure MXene and $BaTiO_3$/MXene composite sensors and the respective NH_3 gas concentration. The fitting functions are $Y = 1.03525X + 1.8036$, $Y = 0.55343X + 0.77445$, and $Y = 1.45588X + 5.42384$, and the correlation coefficients (R^2) are 0.98652, 0.985, and 0.98409, respectively. The detection limit (LOD) of the sensor is the lowest gas concentration that the sensor can distinguish, defined as LOD = 3 σ /*S*, where σ is the root-mean-square deviation of noise, and *S* is the slope of the linear fit curve. According to the measured experimental data, the theoretical LOD value of the

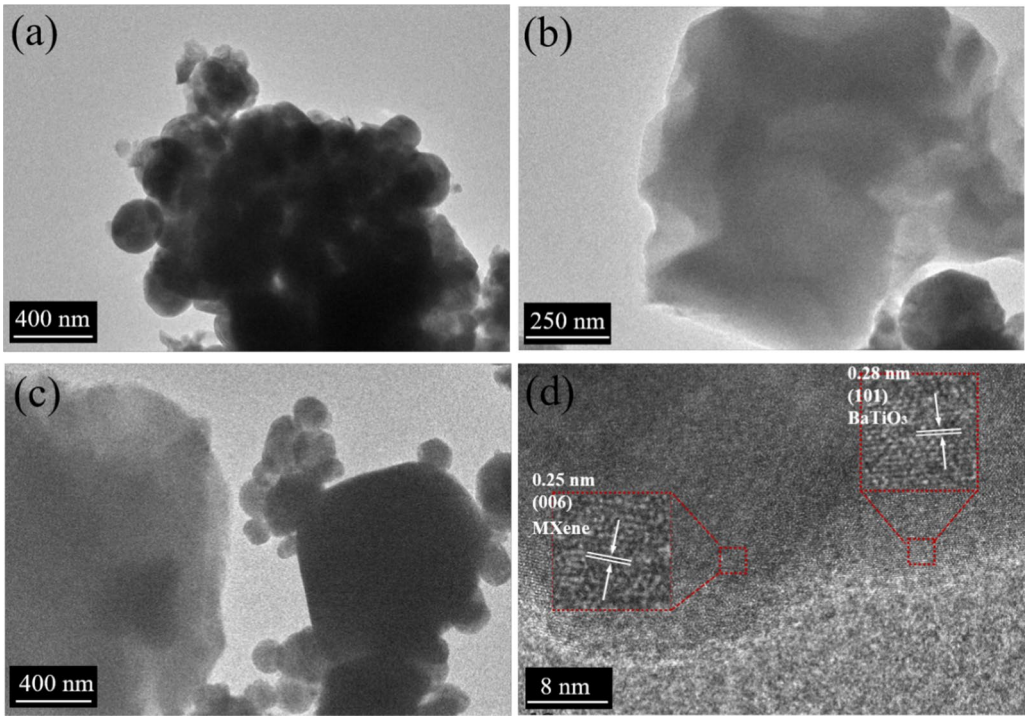

Fig. 4 TEM micrographs of (a) $BaTiO_3$, (b) MXene, and (c) $BaTiO_3$/MXene. (d) HRTEM micrograph of the $BaTiO_3$/MXene composite.

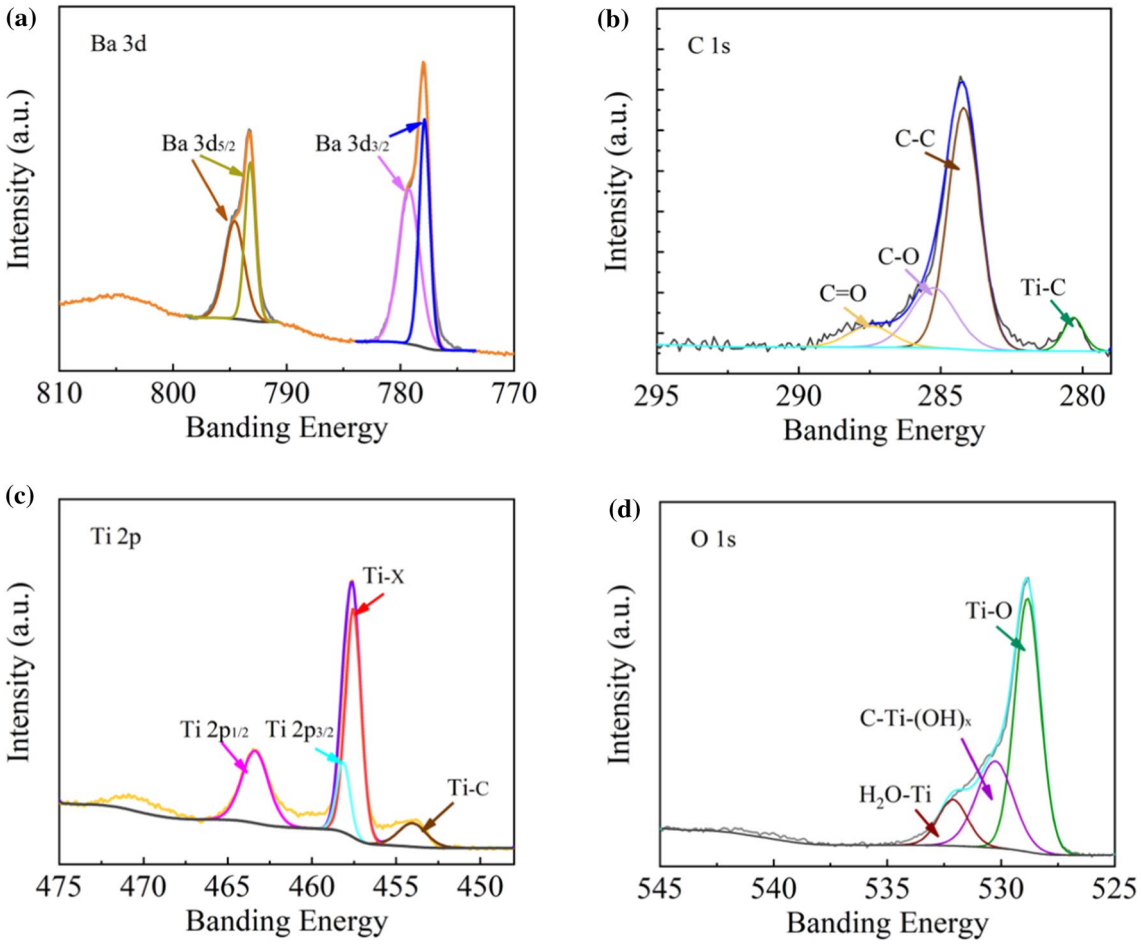

Fig. 5 Core-level XPS spectra of $BaTiO_3$/MXene composite: (a) Ba 3*d*, (b) C 1*s*, (c) Ti 2*p*, and (d) O 1*s*.

$BaTiO_3$/MXene composite sensor for NH_3 is calculated to be 5.41 ppm. In Figure 6c, the response and recovery characteristics of the three sensors to 20 ppm NH_3 are depicted. The response and recovery time of the $BaTiO_3$ sensor, MXene sensor, and $BaTiO_3$/MXene sensor are 27 s/112 s, 55 s/40 s and 40 s/22 s, respectively. The response/recovery times of the $BaTiO_3$/MXene composite sensor are evidently superior to those of the single $BaTiO_3$ or MXene sensors. Obviously, the composite sensor exhibits a quicker detection speed compared to the pristine-material sensor. The $BaTiO_3$ nanospheres within the composite adhere to the accordion-like structure of the MXene, creating an increased number of active adsorption sites, which enhances the absorption and diffusion of NH_3 gas molecules, consequently accelerating the sensor's response and recovery rates.

Figure 7a illustrates the consistent and reproducible nature of the $BaTiO_3$/MXene nanocomposite sensor's responses to NH_3 concentrations of 5 ppm, 10 ppm, and 40 ppm across three consecutive cycles at the same concentration. Figure 7b shows the $BaTiO_3$/MXene composite sensor at 20 ppm NH_3, ethanol (C_2H_6O), carbon monoxide (CO), sulfur dioxide (SO_2), hydrogen sulfide (H_2S) and benzene (C_6H_6). The $BaTiO_3$/MXene nanocomposite sensor was found to be significantly more selective for NH_3 gas than for other types of gases. The results pertaining to the long-term stability measurement of the $BaTiO_3$/MXene nanocomposite sensor after exposure to 5 ppm, 20 ppm, and 40 ppm H_3S are shown in Fig. 7c. The measurement was carried out within a month with an interval of 5 days. The outcomes indicate that the composite sensor exhibits outstanding consistency and enduring stability over time.

Humidity is an important factor affecting the performance of gas sensors. Figure 7d illustrates the difference in the responses of the $BaTiO_3$/MXene-based sensors to 20 ppm NH_3 under various RH. Water droplets evaporate on the heated evaporator within the test chamber, so a hygrometer was employed to continuously monitor the real-time RH within the chamber. Upon reaching the desired humidity level, the evaporation process was halted, followed by the introduction of NH_3 gas for response testing. The NH_3 sensing response was improved in the humidity range of 11–75%, and slightly decreased at 97% RH, indicating a

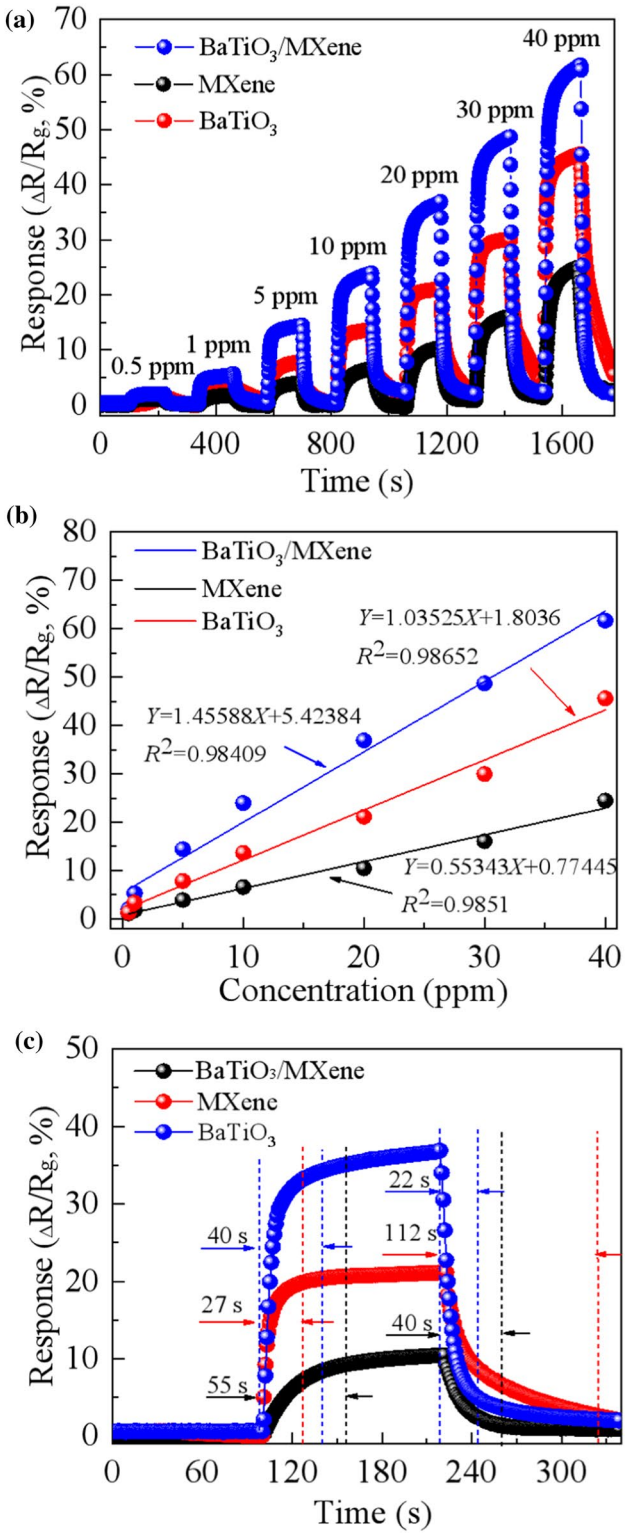

Fig. 6 (a) Responses of $BaTiO_3$, MXene, and $BaTiO_3$/MXene sensors to 1–50 ppm NH_3 gas. (b) Fitting curves of the responses for pristine $BaTiO_3$, MXene, and $BaTiO_3$/MXene sensors to various concentrations of NH_3 gas. (c) Response–recovery curves of pristine $BaTiO_3$, MXene, and $BaTiO_3$/MXene composite sensors for 20 ppm NH_3 gas.

similar phenomenon to the previously reported phenomenon. In general, water molecules play a role in enhancing the adsorption of water-soluble NH_3 on sensitive materials, and the OH^- generated during the water adsorption process has the capacity to capture protons within a humid environment, thereby enhancing the sensor response. In addition, when there are a large number of water molecules on the sensitive material, the active adsorption sites will experience partial occupation, resulting in a decrease in the sensor response.

NH_3 Sensing Mechanism

The changes in resistance observed in the sensing material can be attributed to two distinct mechanisms: firstly, the chemical adsorption of oxygen, and, secondly, the direct transfer of charges. These alterations in resistance are a consequence of the dynamic interplay between these two fundamental processes. On the one hand, the material undergoes chemical adsorption as oxygen molecules adhere to its surface, influencing the overall conductivity. On the other hand, the direct transfer of charges involves the movement of electrical charges within the material itself, further contributing to the observed variations in resistance. This nuanced modulation in resistance is intricately linked to the dual effects of chemical adsorption and charge transfer, underscoring the complex nature of the sensing material's response to external stimuli.[37,38] Figure 8a shows a schematic of the gas sensing mechanism; at ambient temperature, oxygen molecules adsorb to the surface of the $BaTiO_3$/MXene composite to form oxygen anions [O_2^-(ads)] by reacting with electrons in the composite's conduction band, as shown in Eq. 1. As shown in Fig. 8b, the presence of oxygen molecules results in the creation of an electron-depleted layer, causing an increase in resistance. The composite sensor is placed in NH_3, and the adsorbed NH_3 reacts with O_2^-(ads) to generate electrons and release them back to the composite conduction band, as shown in Eq. (2). The aforementioned reaction leads to a decrease in the electron depletion layer's width, consequently reducing the sensor's resistance. When the sensor was placed back in the air environment, after displacement of absorbed NH_3 by air, the surface of $BaTiO_3$/MXene was adsorbed by O_2(ads) to regenerate electrons and oxygen ions, and the resistance of the sensor also returned to its initial value. After measurement, the base resistance of MXene, $BaTiO_3$, and $BaTiO_3$/MXene under air environment (25 °C, 33%RH) was 22.20 Ω, 62.08 MΩ, and 5.10 kΩ, respectively. Obviously, the resistance of the $BaTiO_3$ material after the creation of the composite with MXene is significantly reduced, which may be because the addition of MXene reduces the accumulation of $BaTiO_3$ NPs. The work function of MXene was 4.7 eV, and the band width of $BaTiO_3$ was 3.3 eV.[36,39] MXene has similar electrical conductivity to metals, and electrons will be transferred

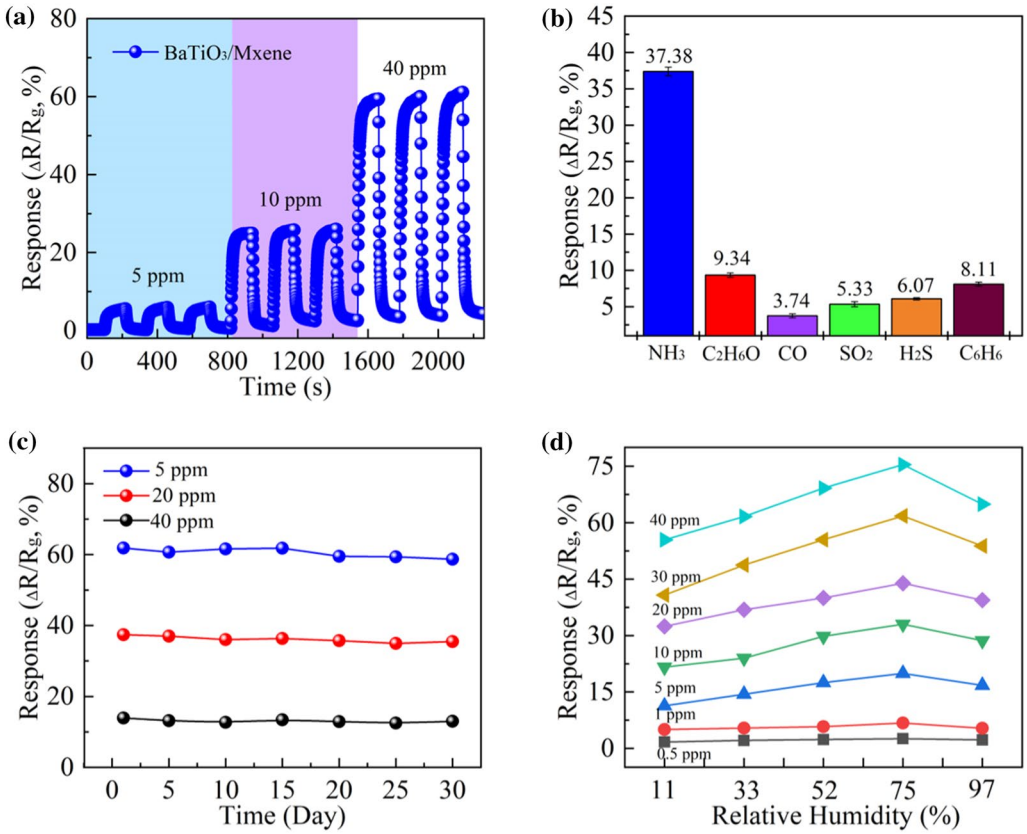

Fig. 7 (a) Repeatability test of $BaTiO_3$/MXene composite sensor for 5, 10, and 30 ppm concentrations of NH_3 gas. (b) Selectivity of $BaTiO_3$/MXene composite sensor for different types of gases with a fixed concentration of 20 ppm. (c) Stability of $BaTiO_3$/MXene composite sensor to 20 ppm NH_3 in 30 days. (d) Moisture resistance test of $BaTiO_3$/MXene composite sensor.

from $BaTiO_3$ to the MXene when the MXene comes into contact with $BaTiO_3$, as shown in Fig. 8c and d.

$$O_2(gas) + e^- \rightarrow O_2^-(ads) \quad (1)$$

$$4NH_3(gas) + 5O_2^-(ads) \rightarrow 4NO(gas) + 6H_2O + 5e^- \quad (2)$$

The gas sensing mechanism of the $BaTiO_3$/MXene composite involves a complex interplay of processes. At its core is a redox reaction, where the composite undergoes chemical transformations in response to the analyte. Concurrently, there is a dynamic exchange of charges between the $BaTiO_3$/MXene composite and the analyte, influencing the material's conductivity. Adding to this, a synergistic effect enhances the gas sensing behavior, showing an amplified response arising from the collaborative action of $BaTiO_3$ and MXene components within the composite. In summary, the gas-sensing mechanism is intricately woven with redox reactions, charge transfer, and cooperative effects, highlighting the sophisticated nature of the $BaTiO_3$/MXene composite in detecting analytes.[40–43]

In the experimental setup, NH_3, serving as the electron donor gas, was utilized, and noteworthy *p*-type sensing behavior towards this reducing gas was observed in the $Ti_3C_2T_x$ film.[44] The manifestation of *p*-type semiconducting characteristics in $Ti_3C_2T_x$ MXenes can be attributed to the influence of adsorbed molecules, such as water and oxygen. These molecules are introduced during the aluminum etching procedure and play a role as *p*-type dopants for $Ti_3C_2T_x$.[45] This *p*-type sensing behavior exhibited by the $Ti_3C_2T_x$ film in response to the NH_3 gas is intricately linked to the presence of adsorbed molecules, showing a dynamic interaction between the material and its environment during the aluminum etching process. The introduced water and oxygen molecules act as effective *p*-type dopants, contributing to the observed *p*-type semiconducting behavior in $Ti_3C_2T_x$ MXenes during the gas-sensing experiment. The resistance of the $BaTiO_3$/MXene composite sensor decreases in a certain concentration of the NH_3, showing a similar *p*-type sensing behavior. This is similar to pure MXene, indicating that MXene significantly contributes to the conduction of carriers in gas sensing.[46] Moreover, the metallic conductive nature and elevated mobility of charge

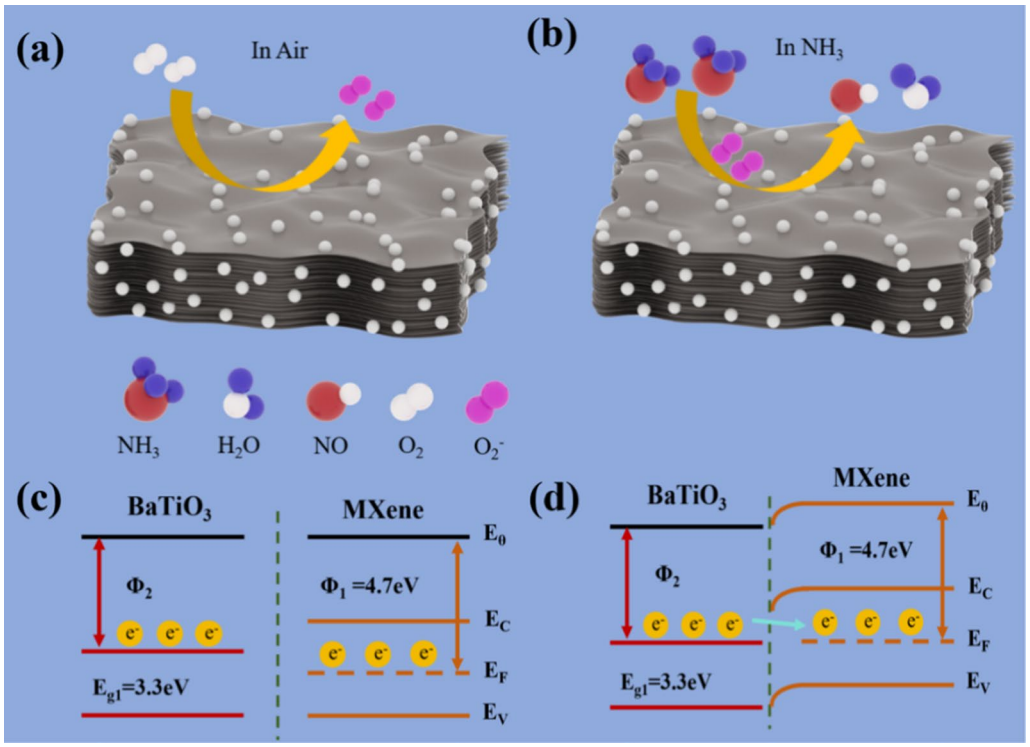

Fig. 8 Schematic of the sensing mechanism of the $BaTiO_3$/MXene composite sensor in air and ammonia gas.

carriers in MXene facilitate prompt charge transfer without necessitating high-temperature activation. This characteristic is also evident in the benefit of gas sensitivity at ambient temperatures in the context of this study.[47]

In this study, the NH_3 sensitivity of MXene nanosheets was significantly improved by compounding $BaTiO_3$ nanospheres. The improved capability in detecting NH_3 can be attributed to the expanded specific surface area of the composite, as well as the augmentation of active sites offered by $BaTiO_3$ and the electronic shift occurring at the interface of the heterojunction contributes to this phenomenon.[48] First, the integration of $BaTiO_3$ nanospheres onto MXene nanosheets was executed, fostering an environment conducive to the permeation and scattering of gas molecules. This synergistic combination not only streamlines the entry and distribution of gas molecules but also enhances the material's receptivity, thereby augmenting its responsiveness. The incorporation of $BaTiO_3$ nanospheres onto the MXene nanosheets creates a symbiotic relationship that optimizes the penetration and dispersion of gas molecules, ultimately leading to an amplification in the material's sensitivity and capacity to respond effectively to external stimuli. This strategic union of $BaTiO_3$ nanospheres with MXene nanosheets serves as a catalyst for elevating the overall performance of the composite, accentuating its ability to detect and react to gas molecules with heightened efficiency and precision..[49] Second, the addition of $BaTiO_3$ results in an increased number of active sites on the composite surface, facilitating the adsorption of NH_3 molecules. This addition enhances and diversifies the available sites for NH_3 adsorption on the composite material. The integration of $BaTiO_3$ leads to a greater density of sites capable of attracting and binding with NH_3 molecules, promoting a more comprehensive and efficient adsorption process. This enrichment of active sites through the inclusion of $BaTiO_3$ contributes to an enhanced ability to attract and retain NH_3 molecules, solidifying the composite's efficacy in NH_3 detection through an expanded and refined surface interaction. In addition, when NH_3 molecules are adsorbed onto the $BaTiO_3$/MXene surface by physical adsorption, a direct exchange of charges occurs between NH_3 molecules and the $BaTiO_3$/MXene surface. Surface electrons engage with the NH_3 substance, leading to a rise in the quantity of conducting entities. The large number of charge carriers leads to an increase in the electrical conductivity of the composite.[50] Therefore, the $BaTiO_3$/MXene composite exhibits better sensing performance.

The remarkable selectivity exhibited by the composite sensor towards NH_3 emanates from its superior capability to adsorb energy in comparison to alternative polar molecules, including methane, CO, carbon dioxide, and nitrogen dioxide. This heightened affinity for absorbing energy, particularly pronounced in the case of NH_3, is attributed to the substantial absorption energy associated with this gas. The functional groups present on the surface of $Ti_3C_2T_x$ play

a pivotal role in this phenomenon, as they readily facilitate the absorption of NH_3 molecules. This interaction leads to a substantial increase in the electrical resistance of the composite sensor, underscoring the specificity of its response to NH_3. The heightened absorption energy of NH_3, coupled with the selective affinity of the $Ti_3C_2T_x$ surface functional groups, collectively contribute to the exceptional selectivity observed in the composite sensor's response to NH_3, thereby distinguishing it from other tested polar molecules.[51,52]

Conclusions

NH_3 sensors based on $BaTiO_3$/MXene sensitive films were prepared by etching and a hydrothermal method. The successful preparation of $BaTiO_3$ and MXene was confirmed by XRD analysis. SEM and TEM characterization results demonstrated uniform dispersion of $BaTiO_3$ nanoparticles and MXene nanosheets. Additionally, XPS analysis confirmed that the $BaTiO_3$/MXene composite film was primarily composed of Ba, C, Ti, and O elements. The experimental results of the $BaTiO_3$/MXene gas sensor show that the prepared $BaTiO_3$/MXene composite thin film sensor has high sensitivity to NH_3, and also has effective selectivity, repeatability, and long-term stability. Finally, the sensing mechanism of $BaTiO_3$/MXene composite films for NH_3 is explained in terms of the interaction between the surface oxygen and the target gas, and the increase of the specific surface area and active sites of the composites. This study validates the promising prospects in the advancement of innovative responsive materials, specifically the $BaTiO_3$/MXene composite, for heightened capabilities in detecting NH_3. The research substantiates the potential of these novel substances to evolve and excel in the domain of advanced NH_3 detection.

Acknowledgments This work was supported by the National Natural Science Foundation of China (51777215), the Special Foundation of the Taishan Scholar Project (tsqn202211077), the Shandong Provincial Natural Science Foundation (ZR2023ME118), and the Natural Science Foundation of Qingdao (23-2-1-219-zyyd-jch).

Conflict of interest The authors declare no competing financial interest.

References

1. D. Zhang, Z. Yang, P. Li, M. Pang, and Q. Xue, Flexible self-powered high-performance ammonia sensor based on Au-decorated $MoSe_2$ nanoflowers driven by single layer MoS_2-flake piezoelectric nanogenerator. *Nano Energy* 65, 103974 (2019).
2. T. Ahamad, M. Naushad, and S.M. Alshheri, Fabrication of highly porous N/S doped carbon embedded with CuO/CuS nanoparticles for NH_3 gas sensing. *Mater. Lett.* 268, 127515 (2020).
3. X. Wang, D. Zhang, H. Zhang, L. Gong, Y. Yang, W. Zhao, S. Yu, Y. Yin, and D. Sun, In situ polymerized polyaniline/MXene (V_2C) as building blocks of supercapacitor and ammonia sensor self-powered by electromagnetic-triboelectric hybrid generator. *Nano Energy* 88, 106242 (2021).
4. D. Zhang, S. Yu, X. Wang, J. Huang, W. Pan, J. Zhang, and J. Zeng, UV illumination-enhanced ultrasensitive ammonia gas sensor based on (001)TiO_2/MXene heterostructure for food spoilage detection. *J. Hazard. Mater.* 423, 127160 (2022).
5. S.J. Gai, B. Wang, X.L. Wang, R.Z. Zhang, S.L. Miao, and Y.Q. Wu, Ultrafast NH_3 gas sensor based on phthalocyanine-optimized non-covalent hybrid of carbon nanotubes with pyrrol. *Sens. Actuators B, Chem.* 357, 131352 (2022).
6. D.Y. Wang, D.Z. Zhang, Y. Yang, Q. Mi, J.H. Zhang, and L.D. Yu, Multifunctional latex/polytetrafluoroethylene-based triboelectric nanogenerator for self-powered organ-like MXene/metal-organic framework-derived CuO nanohybrid ammonia sensor. *ACS Nano* 15, 2911–2919 (2021).
7. R.P. Patil, S.S. Gaikwad, A.N. Karanjekar, P.K. Khanna, G.H. Jain, V.B. Gaikwad, P.V. More, and N. Bisht, Optimization of strontium-doping concentration in $BaTiO_3$ nanostructures for room temperature NH_3 and NO_2 gas sensing. *Mater. Today Chem.* 16, 100240 (2020).
8. R.P. Patil, C. Hiragond, G.H. Jain, P.K. Khanna, V.B. Gaikwad, and P.V. More, La doped $BaTiO_3$ nanostructures for room temperature sensing of NO_2/NH_3: focus on La concentration and sensing mechanism. *Vacuum* 166, 37–44 (2019).
9. R.P. Patil, S.S. Gaikwad, A.N. Karanjekar, P.K. Khanna, G.H. Jain, V.B. Gaikwad, P.V. More, and N. Bisht, Optimization of strontium- doping concentration in $BaTiO_3$ nanostructures for room temperature NH_3 and NO_2 gas sensing. *Mater. Today Chem.* 16, 100240 (2020).
10. R.L. Fomekong, S.J. You, R. Frohnhoven, T. Ludwig, S. Mathur, and B. Saruhan, Self-decoration of barium titanate with rhodium-NP via a facile co-precipitation route for NO sensing in hot gas environment. *Sens. Actuators B* 338, 129848 (2021).
11. S. Joshi, R.K.C. Balasubramanyam, S.J. Ippolito, Y.M. Sabri, A.E. Kandjani, S.K. Bhargava, and M.V. Sunkara, Straddled band aligned CuO/$BaTiO_3$ heterostructures: role of energetics at nanointerface in improving photocatalytic and CO_2 sensing performance. *ACS Appl. Nano Mater.* 1, 3375–3388 (2018).
12. D. Zhou, Z. Kang, X. Liu, W. Yan, H. Cai, J. Xu, and D. Zhang, High sensitivity ammonia QCM sensor based on ZnO nanoflower assisted cellulose acetate-polyaniline composite nanofibers. *Sens. Actuators B, Chem.* 392, 134072 (2023).
13. H.M. Huang, H.Y. Li, X.X. Wang, and X. Guo, Detecting low concentration of H_2S gas by $BaTiO_3$ nanoparticle-based sensors. *Sens. Actuators B* 238, 16–23 (2017).
14. R.P. Patil, P.V. More, G.H. Jain, P.K. Khanna, and V.B. Gaikwad, $BaTiO_3$ nanostructures for H_2S gas sensor: influence of band-gap, size and shape on sensing mechanism. *Vacuum* 146, 455–546 (2017).
15. M. Alhabeb, K. Maleski, B. Anasori, P. Lelyukh, L. Clark, S. Sin, and Y. Gogotsi, Guidelines for synthesis and processing of 2D titanium carbide ($Ti_3C_2T_x$ MXene). *Chem. Mater.* 29, 7633–7644 (2017).
16. M. Hu, T. Hu, Z. Li, Y. Yang, R. Cheng, J. Yang, C. Cui, and X. Wang, Surface functional groups and interlayer water determine the electrochemical capacitance of $Ti_3C_2T_x$ MXene. *ACS Nano* 12, 3578–3586 (2018).
17. J. Pang, R.G. Mendes, A. Bachmatiuk, L. Zhao, H.Q. Ta, T. Gemming, H. Liu, Z.F. Liu, and M.H. Rummeli, Applications of 2D MXenes in energy conversion and storage systems. *Chem. Soc. Rev.* 48, 72–133 (2019).
18. H.J. Koh, S.J. Kim, K. Maleski, S.Y. Cho, Y.J. Kim, C.W. Ahn, Y. Gogotsi, and H.T. Jung, Enhanced selectivity of MXene gas sensors through metal ion intercalation: in situ X-ray diffraction study. *ACS Sens.* 4, 1365–1372 (2019).

19. L.Y. Liang, G.J. Han, Y. Li, B. Zhao, B. Zhou, Y.Z. Feng, J.M. Ma, Y.M. Wang, R. Zhang, and C.T. Liu, Promising $Ti_3C_2T_x$ MXene/Ni chain hybrid with excellent electromagnetic wave absorption and shielding capacity. *ACS Appl. Mater. Interfaces* 11, 25399–25409 (2019).
20. L. Jin, C.L. Wu, K. Wei, L.F. He, H. Gao, H.X. Zhang, K. Zhang, A.M. Asiri, K.A. Alamry, L. Yang, and X.F. Chu, Polymeric $Ti_3C_2T_x$ MXene composites for room temperature ammonia sensing. *ACS Appl. Nano Mater.* 3, 12071–12079 (2020).
21. R.X. Deng, B.B. Chen, H.J. Li, K. Zhang, T. Zhang, Y. Yu, and L.X. Song, MXene/Co_3O_4 composite material: stable synthesis and its enhanced broadband microwave absorption. *Appl. Surf. Sci.* 488, 921–930 (2019).
22. N. Li, Y. Jiang, C.H. Zhou, Y. Xiao, B. Meng, Z.Y. Wang, D.Z. Huang, C.Y. Xing, and Z.C. Peng, High-performance humidity sensor based on urchin-like composite of Ti_3C_2 MXene-derived TiO_2 nanowires. *ACS Appl. Mater. Interfaces* 11, 38116–38125 (2019).
23. W. Yuan, K. Yang, H. Peng, F. Li, and F. Yin, A flexible VOCs sensor based on a 3D Mxene framework with a high sensing performance. *J. Mater. Chem.* 6, 18116–18124 (2018).
24. S.J. Kim, H.J. Koh, C.E. Ren, O. Kwon, K. Maleski, S.Y. Cho, B. Anasori, C.K. Kim, Y.K. Choi, J. Kim, Y. Gogotsi, and H.T. Jung, Metallic $Ti_3C_2T_x$ MXene gas sensors with ultrahigh signal-to-noise ratio. *ACS Nano* 12, 986–993 (2018).
25. S. Chertopalov, and V.N. Mochalin, Environment-sensitive photoresponse of spontaneously partially oxidized Ti_3C_2 MXene thin films. *ACS Nano* 12, 6109–6116 (2018).
26. K. Sukwoo, A. Mirzaei, K.Y. Shin, W. Oum, S.S. Kim, and H.W. Kim, Hyoun Woo Kim, Highly selective NO_2 gas sensing with SnO_2-$Ti_3C_2T_x$ nanocomposites synthesized via the microwave process. *Sens. Actuators B Chem.* 375, 132882 (2023).
27. M. Liu, Y. Ding, Z. Lu, P. Song, and Q. Wang, Layered $Ti_3C_2T_x$ MXene/CuO spindles composites for NH_3 detection at room-temperature. *J. Alloy. Compd.* 938, 168563 (2023).
28. H.F. Zhang, L. Wang, Y.C. Zou, Y.Z. Li, J.Y. Xuan, X.M. Wang, F.C. Jia, G.C. Yin, and M.L. Sun, Enhanced ammonia sensing response based on Pt-decorated $Ti_3C_2T_x/TiO_2$ composite at room temperature. *Nanotechnology* 34, 205501 (2023).
29. M. Taheripour, N. Yasrebi, S. Nasresfahani, and M.H. Sheikhi, Highly sensitive and fast-response volatile organic compounds sensors based on star-shaped $BaTiO_3$/ZnO heterostructures. *IEEE Sens. J.* 21, 4225–4232 (2021).
30. S.K. Hodak, T. Supasai, and J.H. Hodak, Design of low cost gas sensor based on $SrTiO_3$ and $BaTiO_3$ films. *J. Nanosci. Nanotechnol.* 10, 7236–7238 (2010).
31. D.Z. Zhang, Q. Mi, D.Y. Wang, and T.T. Li, MXene/Co_3O_4 composite based formaldehyde sensor driven by ZnO/MXene nanowire arrays piezoelectric nanogenerator. *Sens. Actuators B* 339, 129923 (2021).
32. S. Joshi, S.J. Ippolito, S. Periasamy, Y.M. Sabri, and M.V. Sunkara, Efficient heterostructures of Ag@CuO/$BaTiO_3$ for low-temperature CO_2 gas detection: assessing the role of nanointerfaces during sensing by operando DRIFTS technique. *ACS Appl. Mater. Interfaces* 9, 27014–27026 (2017).
33. H.H. Wang, Z.Q. Guo, W.T. Hao, L. Sun, Y.J. Zhang, and E.S. Cao, Ethanol sensing characteristics of $BaTiO_3/LaFeO_3$ nanocomposite. *Mater. Lett.* 234, 40–44 (2019).
34. Y.H. Wang, Y. Zhou, and Y.J. Wang, Humidity activated ionic-conduction formaldehyde sensing of reduced graphene oxide decorated nitrogen-doped MXene/titanium dioxide composite film. *Sens. Actuators B* 323, 128695 (2020).
35. S.H. Lee, W. Eom, H. Shin, R.B. Ambade, J.H. Bang, H.W. Kim, and T.H. Han, Room-temperature, highly durable $Ti_3C_2T_x$ MXene/grapheme hybrid fibers for NH_3 gas sensing. *ACS Appl. Mater. Interfaces* 12, 10434–10442 (2020).
36. S. Zou, J. Gao, L.M. Liu, Z.D. Lin, P. Fu, S.G. Wang, and Z. Chen, Enhanced gas sensing properties at low working temperature of iron molybdate/MXene composite. *J. Alloys Compd.* 817, 152785 (2020).
37. Z.J. Yang, A. Liu, C.L. Wang, F.M. Liu, J.M. He, S.Q. Li, J. Wang, R. You, X. Yan, P. Sun, Y. Duan, and G.Y. Lu, Improvement of gas and humidity sensing properties of organ-like MXene by alkaline treatment. *ACS Sens.* 4, 1261–1269 (2019).
38. M. Naguib, O. Mashtalir, M.R. Lukatskaya, B. Dyatkin, C.F. Zhang, V. Presser, Y. Gogotsi, and M.W. Barsoum, One-step synthesis of nanocrystalline transition metal oxides on thin sheets of disordered graphitic carbon by oxidation of MXenes. *Chem. Commun.* 50, 7420 (2014).
39. Z. Li, D. Zhang, X. Wang, X. Liu, Y. Yang, C. Du, J. Guo, and Y. Zhang, Passive and wireless NFC tag-type trimethylamine gas detection based on WO_3/MXene composite sensors. *J. Alloy. Compd.* 939, 168730 (2023).
40. S.B. Sun, M.W. Wang, X.T. Chang, Y.C. Jiang, D.Z. Zhang, D.S. Wang, Y.L. Zhang, and Y.H. Lei, $W_{18}O_{49}/Ti_3C_2T_x$ MXene nanocomposites for highly sensitive acetone gas sensor with low detection limit. *Sens. Actuators B* 304, 127274 (2020).
41. W.N. Zhao, N. Yun, Z.H. Dai, and Y.F. Li, A high-performance trace level acetone sensor using an indispensable $V_4C_3T_x$ MXene. *RSC Adv.* 10, 1261–1270 (2020).
42. S. Zhang, Y.L. Ding, Q. Wang, and P. Song, MOFs-derived In_2O_3/ZnO/$Ti_3C_2T_X$ MXene ternary nanocomposites for ethanol gas sensing at room temperature. *Sens. Actuators B, Chem.* 393, 134122 (2023).
43. S. Zhang, P. Song, J. Sun, Y.L. Ding, and Q. Wang, MoO_3/$Ti_3C_2T_x$ MXene nanocomposites with rapid response for enhanced ethanol-sensing at a low temperature. *Sens. Actuators B, Chem.* 378, 133216 (2023).
44. J. Shen, G. Liu, Y. Ji, Q. Liu, L. Cheng, K.C. Guan, M.C. Zhang, G.P. Liu, J. Xiong, J. Yang, and W.Q. Jin, 2D MXene nanofilms with tunable gas transport channels. *Adv. Funct. Mater.* 28, 1801511 (2018).
45. M. Wu, M. He, Q. Hu, Q.H. Wu, G. Sun, L.L. Xie, Z.Y. Zhang, Z.G. Zhu, and A.G. Zhou, Ti_3C_2 MXene-based sensors with high selectivity for NH_3 detection at room temperature. *ACS Sens.* 4, 2763–2770 (2019).
46. E. Lee, A. VahidMohammadi, B.C. Prorok, Y.S. Yoon, M. Beidaghi, and D.J. Kim, Room temperature gas sensing of two-dimensional titanium carbide (MXene). *ACS Appl. Mater. Interfaces* 9, 37184–37190 (2017).
47. D.C. Zuo, S.C. Song, C.S. An, L.B. Tang, Z.J. He, and J.C. Zheng, Synthesis of sandwich-like structured Sn/SnO_x@MXene composite through in-situ growth for highly reversible lithium storage. *Nano Energy* 62, 401–409 (2019).
48. Z. Qin, Z. Wu, Q. Sun, J. Sun, M. Zhang, F. Chen, D. Zhang, C. Lv, and H. Duan, Dog nose-inspired high-performance ammonia sensor based on biochar/SnO_2 composite. *Carbon* 213, 118297 (2023).
49. L.A. Patil, D.N. Suryawanshi, I.G. Pathan, and D.G. Patil, Effect of firing temperature on gas sensing properties of nanocrystalline perovskite $BaTiO_3$ thin films prepared by spray pyrolysis techniques. *Sens. Actuators B* 195, 643–650 (2014).
50. X.Z. Guo, Y.Q. Ding, D.L. Kuang, Z.L. Wu, X. Sun, B.S. Du, C.Y. Liang, Y.J. Wu, W.J. Qu, L. Xiong, and Y. He, Enhanced ammonia sensing performance based on MXene-$Ti_3C_2T_x$ multilayer nanoflakes functionalized by tungsten trioxide nanoparticles. *J. Colloid Interface Sci.* 595, 6–14 (2021).
51. A. Hermawan, B. Zhang, A. Taufik, Y. Asakura, T. Hasegawa, J. Zhu, P. Shi, and S. Yin, CuO nanoparticles/$Ti_3C_2T_x$ MXene hybrid nanocomposites for detection of toluene gas. *ACS Appl. Nano Mater.* 3, 4755–4766 (2020).

52. Q.H. Wu, G. Sun, L.L. Xie, Z.Y. Zhang, Z.G. Zhu, A.G. Zhou, M. Wu, M. He, and Q.K. Hu, Ti_3C_2 MXene based sensors with high selectivity for NH_3 detection at room-temperature. *ACS Sens.* 4, 2763–2770 (2019).